A USRP-Based GNSS and Interference Signal Generator and Playback System

Ruihui Di[1], Senlin Peng[2], Steve Taylor[1], Yu Morton[1]
[1] Electrical & Computer Engineering Department
Miami University
Oxford, OH 45056 USA
[2] Electrical & Computer Engineering Department
Virginia Tech
Blacksburg, VA 24061 USA

Abstract—**This paper presents a low cost, portable, and flexible GNSS signal and interference signal generator based on a general purpose software radio front end, the Universal Serial Radio Peripheral (USRP) family of devices. We paired a USRP-N210 mother board with appropriate RFX daughter boards to generate all GNSS signals controlled by a personal computer. The source of the signal can be pre-recorded digital samples obtained from specific RF front end or arbitrary samples generated using MATLAB programs. An adjustable low noise signal amplifier mounted between the USRP output and the transmitting antenna was used to control the transmitted power of the signal. A spectrum analyzer was used to directly monitor the transmitted signal. The NovAtel receiver was used to verify the performance of this signal generator and playback system. The received GNSS data after transmitting via USRP-N210 and the original GNSS data before transmitting are processed by NovAtel receiver and software receiver programs respectively for performance evaluation purposes. Some comparisons had been done to demonstrate the accuracy of the playback system.**

Keywords: GNSS; interference signal generator; playback system;

I. INTRODUCTION

GNSS signals are commonly subjected to both manmade and natural interferences such as RF jamming, ionosphere scintillations, multipath, and signal anomaly. In order to achieve the desired navigation application performance, advanced receiver processing or multi-sensor integration algorithms must be developed to mitigate these interferences. A flexible multi-frequency multi-constellation GNSS signal generator is an important enabler of robust GNSS receiver research and development.

There is a growing number of companies that offer high end GNSS signal simulators or generators. One problem of these high end signal simulators or generators is their high costs. Additionally, these instruments can be cumbersome in size. We developed a low cost, portable, and flexible GNSS signal and interference signal generator based on a general purpose software radio front end, the Universal Serial Radio Peripheral (USRP) family of devices. Specifically, we paired a USRP-N210 mother board with appropriate RFX daughter boards to generate all GNSS signals controlled by a personal computer. The source of the signal can be pre-recorded digital samples obtained from specific RF front end or arbitrary samples generated using MATLAB programs. An adjustable low noise signal amplifier mounted between the USRP-N210 output and the transmitting antenna was used to control the transmitted power of the signal. A spectrum analyzer was used to monitor the transmitted signal. The receiver output and the transmitted signal are processed by NovAtel receiver and compared with the original signal parameters to demonstrate the accuracy of the playback system.

The original objective of this project is to generate ionosphere scintillation signals for robust receiver algorithms developments. Ionosphere scintillation can seriously affect GNSS receiver's carrier tracking loop performance. It is a stochastic phenomenon characterized by a wide range of parameters distributions and its occurrences can be difficult to capture. Ref. [1] discussed a GNSS simulator that generates synthetic scintillation time-series based on the GISM model [2]. It is well known that a model cannot fully characterize the highly dynamic and variable nature of ionosphere scintillations. A more flexible signal generator with real scintillation RF signal playback capability as well as software controlled synthetic scintillation signals is more desirable.

In the past four years, an ionosphere scintillation monitoring and data collection system has been established in Alaska to collect both processed and raw RF samples for GPS and GLONASS signals during scintillations [3]. These data contains varying levels of scintillation events and can be directly used or modified as real scintillation signal sources. Dynamic synthetic scintillation signals can be generated using existing known models [4][5] or new models based on recent scintillation data analysis results.

This original objective has been extended to include the generation of multipath and interferences. This extension is motivated by the numerous observations of scintillation signals co-existing with multipath and the need to distinguish between scintillation and interferences [6][7].

978-1-4673-0387-3/12/$31.00 ©2012 IEEE

II. USRP-N210 RF FRONT END ARCHITECTURE AND DIGITAL SIGNAL PROCESSING

The basic designing philosophy of USRP is that all waveforms processing operation will be completed on the host CPU, such as modulation and demodulation. All other operations, such as digital down conversion, sampling and interpolation and other high-speed general-purpose operation will be completed on the FPGA board. Fig.1 is the block schematic diagram of digital signal processing on USRP-N210 FPGA board. The RF signal received by the antenna will first undergo a low IF-based pre-processing unit which combines the traditional super-heterodyne and analog complex down-conversion technology as shown in Fig.2 [8]. After pre-processing, the analog data will pass through the ADC units where the signal will be sampled with the sampling rate f_s. The digital signal down-conversion process will be completed in the FPGA (shown inside the red dashed line area). When the bandwidth decimation factor is N, the sample rate of the output digital signal after passing through the decimating low pass filter is f_s/N. The decimated digital signal which is consisted of I and Q with 16 bit resolution will be transferred to the host PC via the Gigabit Ethernet interface.

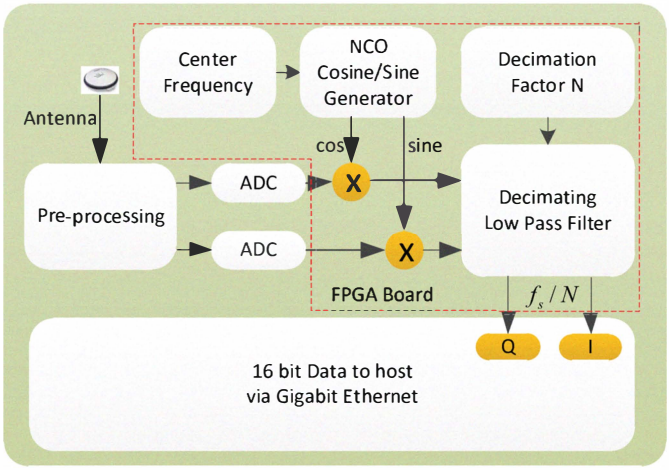

Fig.1. Block Schematic Diagram of Digital Signal Processing on FPGA Board

The above information describes the data processing when the USRP-N210 used as receivers. When the USRP-N210 used in transmitting mode (transmitter), the implementation is a fully reversed process.

Compared to the first generation product, USRP-N210 offers higher speed, better performance, and increased flexibility [9], and is therefore used in our project. The Universal Hardware Driver (UHD) which is supported on Linux operating systems is becoming the official driver for the USRP-N210. In this project, the UHD is successfully installed and working properly on the Ubuntu 11.04 Linux operating system. Some key components differences among the USRP-N210, USRP2 and USRP are listed in TABLE Ⅰ.

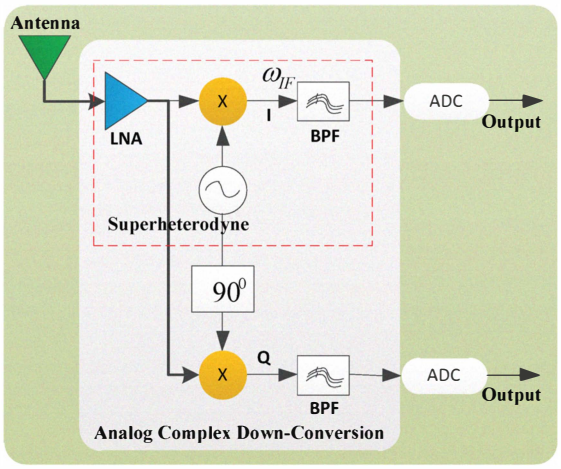

Fig.2. Signal Down-conversion Architecture (from Ref. [8])

TABLE I: KEY COMPONENTS DIFFERENCES AMONG USRP-N210, USRP2 AND USRP [9]

Components	USRP-N210	USRP2	USRP
RF Range	0~5.9GHz		
FPGA	Xilinx Spartan 3A	Xilinx Spartan 3-2000	Altera Cyclone
DACs	Two 400MS/s 16-bit		4 128MS/s 14-bit
ADCs	Two 100MS/s 14-bit		4 64MS/s 12-bit
Sampling Freq.	50MHz		16MHz
PC Connect.	Gigabit Ethernet		USB 2.0

TABLE II: CURRENT AVAILABLE DAUGHTER BOARDS [10]

Name	Available Freq.	Function
BasicRX	1-250 MHz	Receiver
BasicTX	1-250 MHz	transmitter
LFRX	DC-30 MHz	Receiver
LFTX	DC-30 MHz	transmitter
TVRX2	50-860 MHz	receiver
DBSRX2	800MHz-2350 MHz	receiver
WBX	50 MHz to 2.2 GHz	Transceiver
SBX	400 MHz to 4.4 GHz	Transceiver
RFX900	750MHz-1050 MHz	Transceiver
RFX1200	1150MHz-1450 MHz	Transceiver
RFX1800	1500MHz-2100 MHz	Transceiver
RFX2400	2300MHz-2900 MHz	Transceiver
XCVR2450	2.4-2.5 GHz &4.9-5.9 GHz	Transceiver

Paired with specific daughter boards, the USRP-N210 is capable of processing signals from DC to 5.9GHz. TABLE Ⅱ lists the current available daughter boards that can be used for radio frequency signal processing. The RFX1800 (1500 MHz-2100 MHz) covers GPS and GLONASS L1 band, while RFX1200 (1150 MHz -1450 MHz) covers the GPS L2 and L5 and GLONASS L2 band. In our project, we select both

RFX1800 and RFX1200 daughter boards to receive and transmit the GPS and GLONASS signals.

III. GNSS SIGNAL SIMULATION AND REAL DATA COLLECTION

In our project, both the simulated GNSS data and the real GNSS data that received via the GNSS signal front end were used to verify the performance of this USRP-N210 based signal generator and play back system. The GPS L1, L2C, L5, and GLONASS signal generation structure characteristics were summarized. The real GNSS signal collection system in Miami University is also introduced herein.

A). GPS SIGNAL GENERATION

The polynomials and signal structures to generate GPS L1, L2C are completely described in GPS Interface Control Document (ICD-GPS-200C). The description of the new GPS L5 signal is also available in IS-GPS-705. The GPS signal modulation format at L1 and L2C are shown by Fig.3, 4, and 5 respectively.

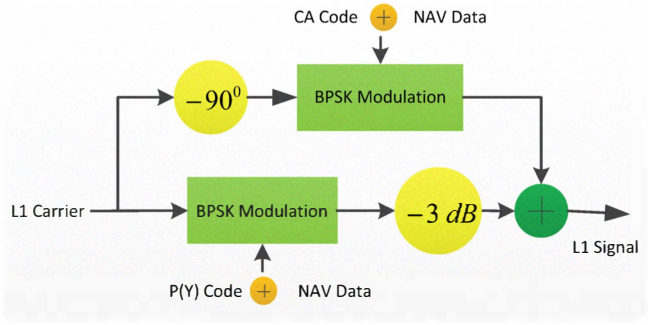

Fig.3. GPS Signal Modulation Format at L1

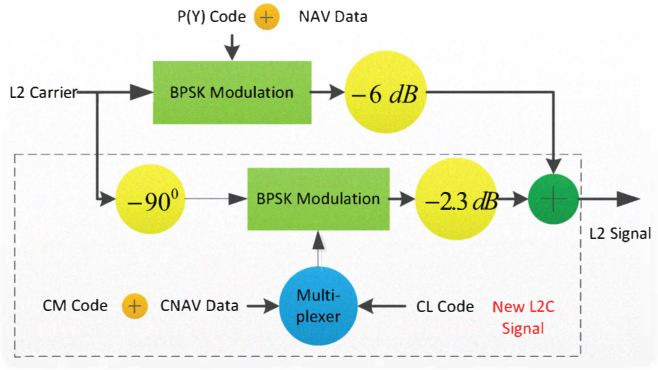

Fig.4. GPS Signal Modulation Format at L2

The general expression for L1 and L2 signal are given by:

$$s_{L1}^{(k)}(t)=\sqrt{2P_C}*C^{(k)}(t)*D^{(k)}(t)*\cos(2\pi f_{L1}t+\theta_{L1}) + \sqrt{2P_{Y1}}*P^{(k)}(t)*D^{(k)}(t)*\sin(2\pi f_{L1}t+\theta_{L1}) \quad (1)$$

$$s_{L2}^{(k)}(t)=\sqrt{2P_{Y2}}*P^{(k)}(t)*D^{(k)}(t)*\sin(2\pi f_{L2}t+\theta_{L2}) \quad (2)$$

where P_c, P_{Y1} are the signal powers for L1 signals; P_{Y2} is the signal power for L2 signals; $C^{(k)}$ and $P^{(k)}$ are the C/A code and P(Y) code sequences assigned to the satellite number k; $D^{(k)}$ are the satellite navigation data bit stream; f_{L1} and f_{L2} are the carrier center frequencies corresponding to L1 and L2 respectively; θ_{L1} and θ_{L2} are the phase offsets for L1 and L2 signals respectively [11].

The general expression for L2C signal is given by:

$$s_{L2}^{(k)}(t)=\sqrt{2P_{C2}}*D_{C2}^{(k)}(t)*CM^{(k)}(t)*\cos(2\pi f_{L2}t+\theta_{L2}), \quad nT_{C2}<t\le(n+1/2)T_{C2} \quad (3)$$

$$s_{L2}^{(k)}(t)=\sqrt{2P_{C2}}*CL^{(k)}(t)*\cos(2\pi f_{L2}t+\theta_{L2}), \quad (n+1/2)T_{C2}<t\le(n+1)T_{C2} \quad (4)$$

where CM is the moderate-length code for the kth satellite; CL is the long code for kth satellite; T_{C2} is the chip width; the superscript (k) indicates the kth satellite. The new L2C signal generation is shown by Fig.4.

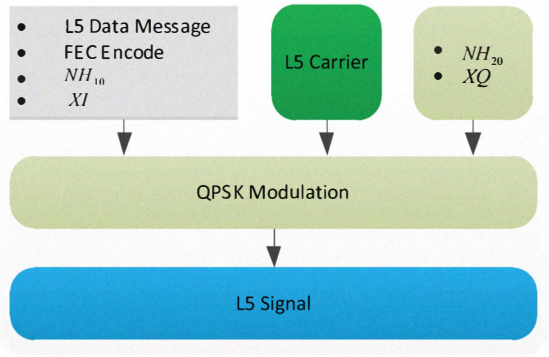

Fig.5. Block Diagram of GPS L5 Signal Generation

The general expression for L5 signal is given by:

$$s(t)=\sqrt{2P_{L5}}[D_{L5}^{(k)}(t)*XI(t)*NH_{10}(t)*\cos(2\pi(f_{L5}+f_d)*t+\theta_{L5}) + XQ(t)*NH_{20}(t)*\sin(2\pi(f_{L5}+f_d)*t+\theta_{L5})] \quad (5)$$

where P_{L5} is the total power of the received GPS L5 signal, D(t) is the binary Non-Return to Zero (NRZ) navigation message, XI(t) and XQ(t) are the binary PRN code, NH_{10} and NH_{20} are the 10-bit and 20-bit Neuman-Hoffman (NH) code respectively, f_{L5} is the L5 carrier frequency, f_d is the Doppler frequency due to the relative motion between the satellite and the receiver, θ_{L5} is the carrier phase delay. Fig.5 shows the block diagram for the GPS L5 signal generation.

B). GLONASS SIGNAL GENERATION

Unlike GPS which uses code division multiple access (CDMA) technology, the GLONASS uses frequency division multiple access (FDMA) modulation technology. The carrier frequency for each GLONASS satellite is defined by the following equation [11]:

$$f_K = 1.602GHz + K \times 562.5kHz, K = -7,-6\cdots 13 \quad (6)$$

where f_K is the carrier frequency, K is the GLONASS channel number which ranges from -7 to 13 including 0.

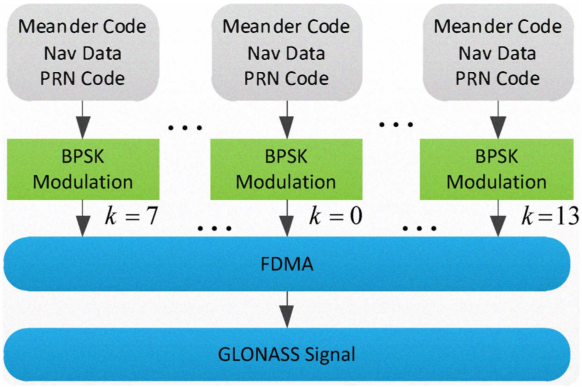

Fig.6. Block Schematic Diagram of GLONASS Signal Generation

Fig.6 shows the diagram for the GLONASS signal generation. The modulo-2 operation was carried out among the meander code, navigation data and PRN code. Then the modulo-2 result modulates onto the GLONASS L1 sub-carrier. The PRN code has a chipping rate of 511 KHz chips and 1 ms in period. The polynomial for generating the GLONASS PRN code is given as follows [12]:

$$X = 1 + x^5 + x^9 \quad (7)$$

C). REAL GNSS DATA COLLECTION

Besides the simulated GNSS signal data, we can collect the real GNSS signal data via a specific GNSS signal front end. Fig.7 shows the data receiving instrument configuration which was set up in the Software Receiver Lab at Miami University. The real RF GNSS signal first impinged on the NovAtel GPS-703-GGG antenna, which is an active antenna. The antenna is connected with a 4-way splitter followed by a TRIGR front end, a NovAtel OEM4 dual frequency hardware receiver, and a USRP-N210 front end. Fig. 8 shows the snapshot of the laboratory setup. One important use of NovAtel OEM4 dual frequency hardware receiver is that it can provide 5 DC volts power supply to power up the NovAtel GPS-703-GGG antenna via the DC port in the 4-way splitter. The TRIGR front end is an instrumentation quality RF front end built at the Ohio University Avionics Engineering Center [13]. It provides simultaneous access to four channels (two GPS L1s, one L2 and one L5). The TRIGR front end works at a fixed sampling frequency of 56.32MHz and IF frequency at 13.68MHz with configurable bit resolution at 2, 4, 8, and 16. The sampling frequency of USRP-N210 can be set manually, such as we can set the frequency at 5MHz or 8MHz for GPS L1 and L2C and 20MHz for GPS L5 and GLONASS L1 signals.

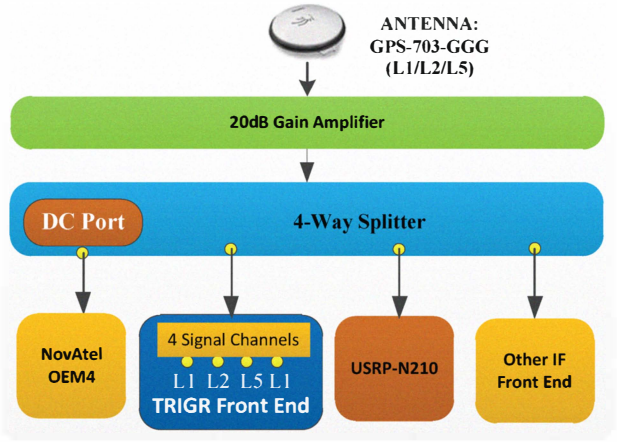

Fig.7. Block Diagram of Real GNSS Data Collection System at Miami University

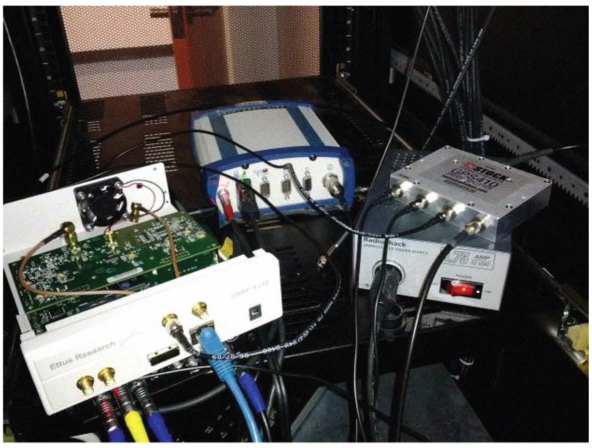

Fig.8. Snapshot of the Real Data Collection System

IV. PLAYBACK SYSTEM PERFORMANCE ANALYSIS

In order to verify the performance of the signal generator and playback system developed, several experiment cases were carried out. The GPS simulated signals for L1, L2C and L5 signal were used to test the performance of this playback system. The USRP-N210 and RFX1800 and RFX1200 daughter boards were used to transmit and receive the data. Besides the simulated GNSS data, we also used the real GNSS data to test the performance of this playback system.

Case1: Transmit GPS L1 signal with daughter board RFX1800

We selected the GPS PRN18 satellite as the simulated signal with code sampling rate 5MHz and code phase 500 sample points. The simulated Doppler frequency is 2.1 KHz. The carrier

to noise ratio is 49 dB-Hz. The acquisition plot of the simulated PRN 18 is shown by Fig.9.

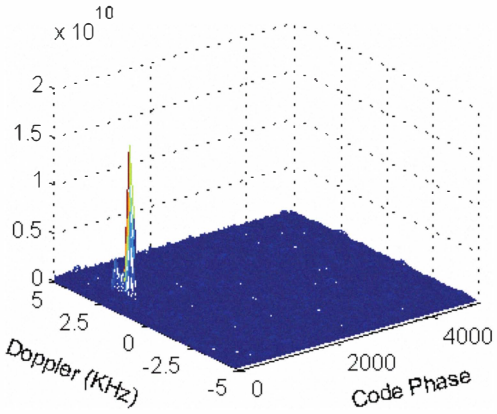

Fig.9. GPS PRN18 Satellite Acquisition Process

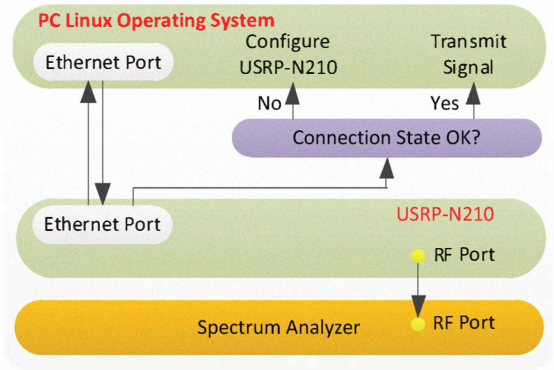

Fig.10. Block Schematic Diagram of USRP-N210 Transmission Process

The block schematic diagram of USRP-N210 transmission process is shown by Fig.10. The UHD environment is installed under Ubuntu 11.04 Linux operating system. The PC and USRP-N210 are connected with each other via the Gigabit Ethernet port. The transceiver daughter board RFX1800 is selected as the transmitting board for GPS L1 signal. We used the Agilent E4404B Spectrum Analyzer to monitor the transmitted signal.

An initialization process is needed to establish communication between the USRP-N210 and the hosting PC before configuration of some specific parameters of the transmitting command. The USRP-N210 can recognize three data types: double, float, and short. In this transmission experiment, we set the data type parameter as short, and the center frequency as 1.57542 GHz, the data sample rate as 5MHz. The spectrum of the original data is shown in Fig.11 while the spectrum analyzer monitor result for transmitting L1 signal is shown as Fig.12.

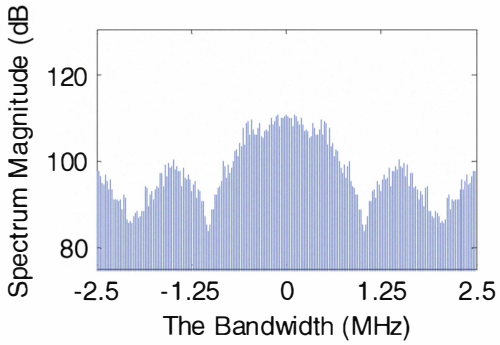

Fig.11. L1 CA Code Spectrum (PRN: 18, Sampling Rate 5MHz)

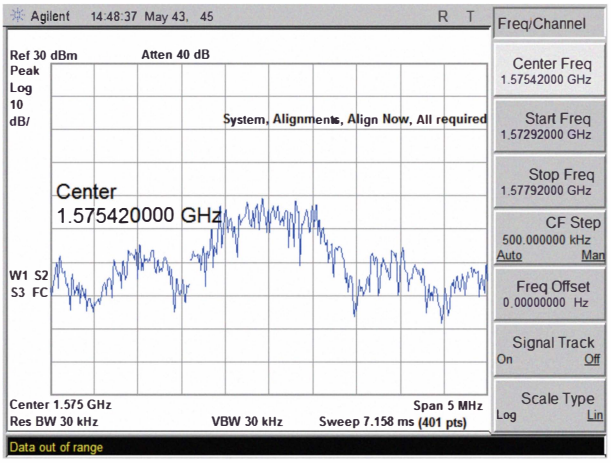

Fig.12. Spectrum Analyzer Monitoring Result of GPS L1 Signal

In comparison with the simulated signal spectrum (Fig.11) and the transmitted signal spectrum which is shown as Fig.12, we can see that the spectrum envelope of both the simulated data and transmitted data agree with each other.

Case2: Transmit GPS L2C and L5 signals with daughter board RFX1200

In this experiment case, the RFX1200 transceiver daughter board is used as the transmitter board. When transmitting L2C signal, we set the transmitting command parameter as follows: transmission carrier center frequency as 1.2276GHz, sample rate as 5MHz, data type as short.

Fig.13 and Fig.14 are the spectrum of simulated input L2C signal data and the transmitted L2C signal via USRP-N210 respectively. According to the two spectrum envelope results, we can also come to the conclusion that they agree with each other very well.

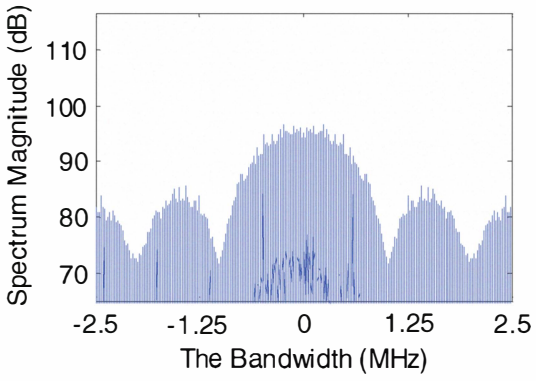

Fig.13. Input GPS L2C Code Spectrum (PRN: 1, Sampling Rate 5MHz)

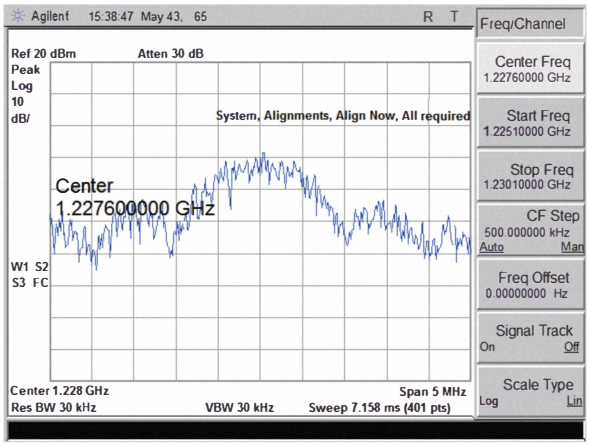

Fig.14. Spectrum Analyzer Monitoring Result of GPS L2C Signal

Accordingly, we can transmit the GPS L5 signal via USRP-N210. The corresponding transmitting parameter that we set in this case is as follows: transmission carrier center frequency as 1.17645GHz, sample rate as 30MHz, data type as short.

Fig.15 is the spectrum of simulated L5 data. Fig.16 is the monitored spectrum of the transmitted L5 signal via USRP-N210. The two spectrum envelope results can also show that they are matches with each other.

Similarly, we can transmit other GNSS signals, such as GLONASS, GALILEO and so on. An adjustable low noise signal amplifier mounted between the USRP-N210 output and the transmitting antenna can be used to control the transmitted power of the signal.

Case3: USRP-N210 to USRP-N210 transmitting and receiving experiment

In this experiment case, we used two USRP-N210 units: one as the transmitter, the other as the receiver to receive the data transmitted from the transmitter. Each unit is controlled by a PC with Linux operating system.

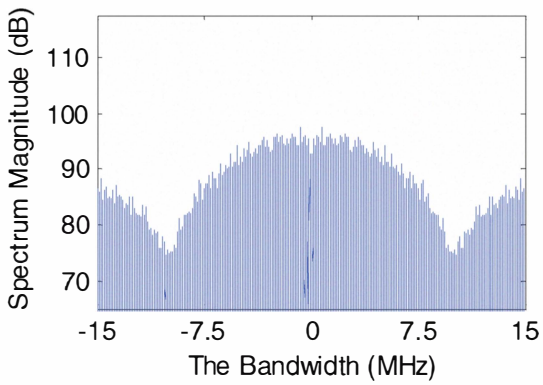

Fig.15. L5 Code Spectrum (Sampling Rate 30MHz)

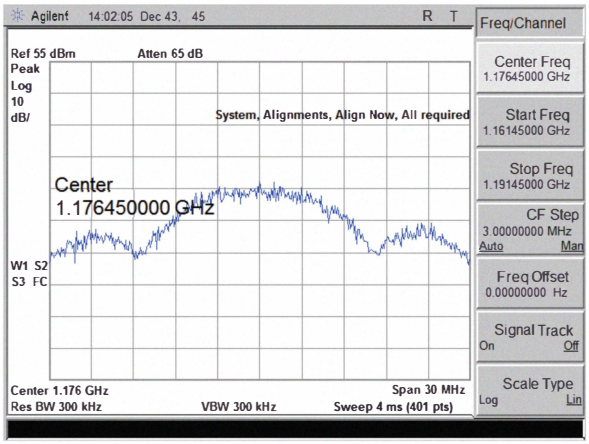

Fig.16. Spectrum Analyzer Monitor Result of L5 Signal

Fig.17. Snapshot of USRP-N210 to USRP-N210

Fig.17 is a snapshot which shows the USRP-N210 to USRP-N210 transmitting and receiving system. Fig.18 is the block schematic diagram of USRP-N210 to USRP-N210 transmitting and receiving process. Each USRP-N210 has the RFX1800 daughter board mounted on it. In the signal transmitting computer side, we set the transmitting parameters as follows: transmission carrier center frequency as 1.57542GHz, sample

rate as 5MHz, data type as short. We choose the GPS L1 signal as the source data used in Case1. In the signal receiving computer side, we set the receiving parameters as follows: carrier center frequency as 1.57542GHz, sample rate as 5MHz, data type as short.

The spectrum of both the transmitted and received data are shown by Fig.19 and Fig.20 respectively. According to the two spectrum results, we can come to the same conclusion that the spectrum envelopes of both the transmitted and received data are nearly the same with each other.

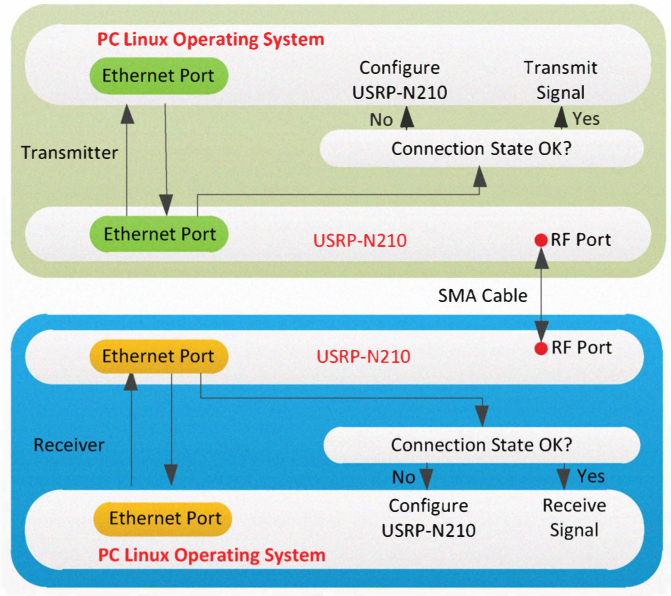

Fig.18. Block Schematic Diagram of USRP-N210 to USRP-N210 Transmitting and Receiving Process

Case4: Real GNSS Data Playback via USRP-N210 and NovAtel Receiver

Repeated experimental cases demonstrated that the envelope are nearly the same between the simulate signal's spectrum and the monitored spectrum result of the spectrum analyzer. To further verify the performance of the playback system, we used the GNSS data received via a real GNSS front end as input for testing.

In this experiment case, the real GPS L1 signal data was chosen as the transmitted source data with sampling rate 5MHz. Fig.21 shows the block schematic diagram of playback system with USRP-N210 and NovAtel receiver. The personal computer1 (PC1) in the upper side of Fig.21 acts as the controller which is used to control the USRP-N210. In the lower side of Fig.21, the personal computer2 (PC2) is used as the monitor which can directly monitor the output result of the NovAtel receiver. The PC1 connects the USRP-N210 via the Ethernet port. The PC2 connects the NovAtel receiver via the serial port (RS-232).

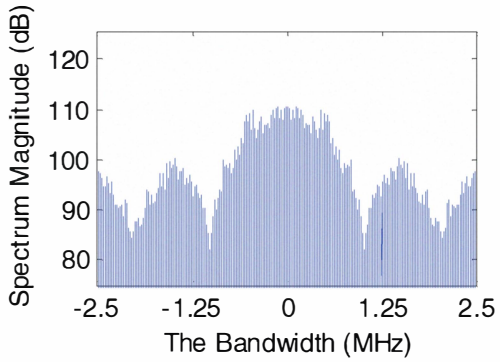

Fig.19. L1 CA code Spectrum (PRN: 18, Sample rate 5MHz)

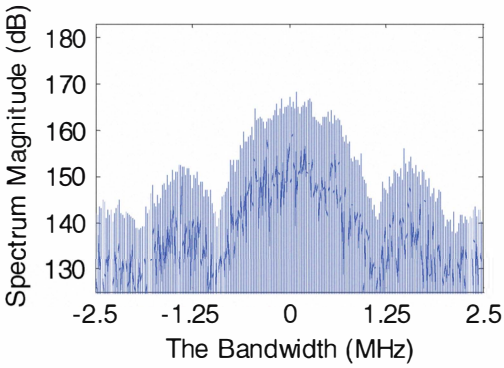

Fig.20. L1 CA Code Spectrum after Receiving via USRP-N210 (Sampling rate 5MHz)

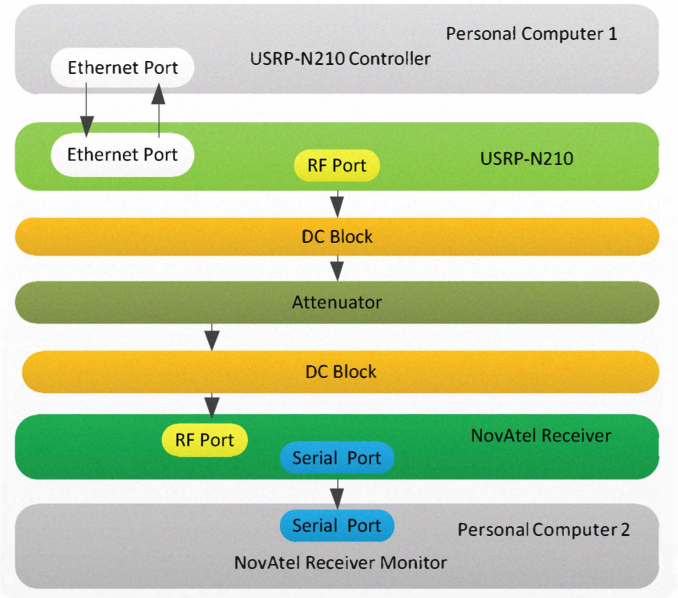

Fig.21. Block Schematic Diagram of Playback System with USRP-N210 and NovAtel Receiver

Note that both the USRP-N210 and NovAtel receiver can output DC voltage, the DC block unit after the output of the USRP-N210 and before the input of the NovAtel receiver are needed to protect the units. Between the two DC blocks, we used 75 dB attenuator and a 1 meter cable line to connect the USRP-N210 and NovAtel receiver to ensure sufficient attenuation of the playback system output so that the NovAtel receiver input is not saturated. The snapshot of experimental setup is shown in Fig.22.

Fig.22. Snapshot of USRP-N210 and NovAtel Receiver in the Playback System

Fig.23-25 shows the Novatel receiver outputs. Fig.23 indicates that 6 satellites were acquired: PRN 25, 31, 12, 14, 22, 18. The sky plot of satellites is shown as Fig.24. The user position information is also calculated by NovAtel Receiver and is shown in Fig.25.

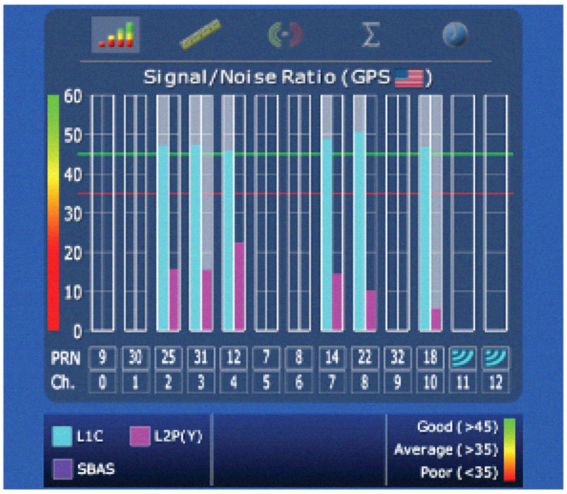

Fig.23. Signal to Noise Ratio Monitored by NovAtel Receiver

Software receiver algorithms are used to process the original data. TABLE III shows the C/N_0 computed by the software algorithms for the input signal and the Novatel receiver generated output signal-to-noise ratio (SNR). Notice that PRN 11 does not appeared in the Sky-plot of the satellites monitored by NovAtel receiver and therefore does not have an entry of SNR value in the table. The software receiver calculation shows that PRN 11 has the smallest C/N_0 in the input and has a low elevation. All other 6 satellites successfully monitored by NovAtel receiver are all above 30 degrees in elevation angles. There are several possible reasons that PRN11 is not detected by the NovAtel receiver. One reason is that the USRP-N210 as a transmitter can also induce additional noise when transmitting the GNSS original data. Another reason is that when the GNSS signal in low elevation angle, there are much complex signal environment exist, such as multi-path, noise etc., which makes the NovAtel receiver very hard to monitor those low elevation angle satellites.

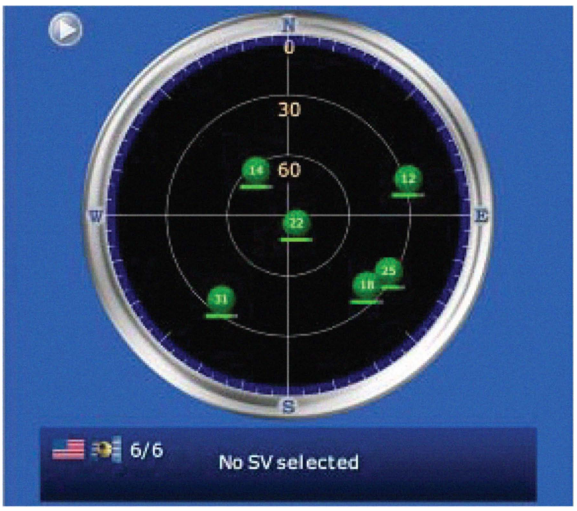

Fig.24. Sky Plot of Satellites Monitored by NovAtel Receiver

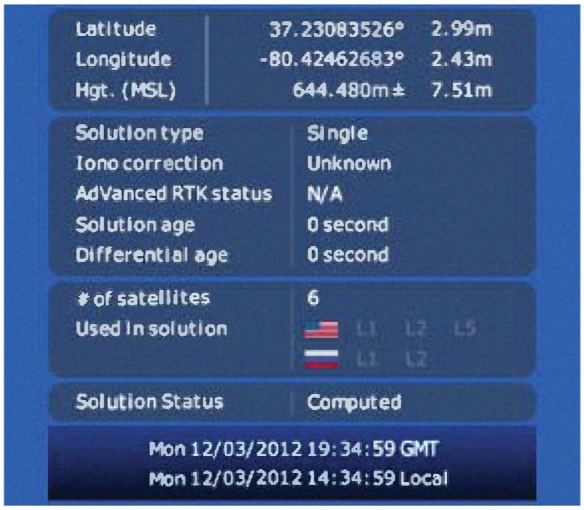

Fig.25. Position Information Monitored by NovAtel Receiver

Comparison of absolute SNR for the input signal generated by our software algorithm and the CNR for the output signal generated by the NovAtel receiver can be misleading as the specific approaches used in the calculation can be very different. Nevertheless, we can examine the relative differences in each set

of results and see if any consistency exists between the two sets of data. We select PRN 12 as our reference satellite and compute the difference between other satellite and PRN 12. The results are also listed in Table III.

TABLE III: RESULTS PROCESSED BY SOFTWARE RECEIVER AND NOVATEL RECEIVER

Processed by Software Receiver			**Monitored by NovAtel Receiver**		
PRN	SNR (dB)	ΔSNR (dB)	PRN	CNR (dB-Hz)	ΔCNR (dB-Hz)
11	12.2				
12	13.6		12	45.5	
14	16.7	3.1	14	48.5	3.0
18	13.3	-0.3	18	46.6	1.1
22	18.6	5.0	22	50.4	4.9
25	13.9	0.3	25	47.2	1.7
31	13.7	0.1	31	47.1	1.6

V. CONCLUSIONS

Several experiments cases with respect to signal transmitting and receiving were successfully carried out and described in the previous sections of this paper. All these experiment results show that we can generate all GNSS signals controlled by a computer based on USRP-N210 paired with appropriate daughter boards (such as: RFX1800, RFX1200, etc.). The source of the signals can be pre-recorded digital samples obtained from specific GNSS RF front end or arbitrary samples generated using MATLAB programs. Such a low cost, portable, and flexible GNSS signal and interference signal generator can help us doing research in many academic fields, such as signal anti-jamming, weak signal acquisition and tracking, ionosphere scintillation research, etc. It can also be a good reference for engineers and researchers doing research in engineering and academic researching fields. The results show that the two sets of data are consistent with each other with about 1 dB fluctuations.

ACKNOWLEDGMENTS

This project is supported by Miami University Office for Advancement of Research and Scholarship.

REFERENCES

[1]. R. Prieto-Cerdeira, R. Orus, "Testing ionospheric scintillation monitors based on GNSS using Spirent constellation simulator," Proc. 2011 Ionospheric Effect Symposium, Alexandria, VA, May 2011.

[2]. Y. Beniguel and P. Hamel, "A global ionosphere scintillation propagation model for equatorial regions," J. Space Weather Space Clim., DOI: 10.1051/swsc/2011004, A04, 2011.

[3]. W. Pelgrum, Y. Morton, F. van Graas, P. vikram, S. Peng, "Multi-domain analysis of the impact of natural and man-made ionosphere scintillations on GNSS signal propagation," Proc. ION GNSS, Portland, OR, Sept. 2011.

[4]. Humphreys, T. E., M. L. Psiaki, and P. M. Kintner, Jr., "Modeling the effects of ionospheric scintillation on GPS carrier phase tracking," IEEE Trans. Aeros. Elec. Sys., Vol.46, Issue 4, p1624-1637, Oct. 2010.

[5]. Pullen, S., Opshaug, G., Hansen, A., et al., "A Preliminary Study of the Effect of Ionospheric Scintillation on WAAS User Availability in Equatorial Regions", Proc. ION GPS, Nashville, TN, Sept. 1998.

[6]. Vikram, P., Y. Morton, W. Pelgrum, "An event driven GPS data collection system for studing ionospheric scintillation," Proc. ION GNSS, Portland, OR, Sept. 2011.

[7]. Vikram, P., "Event driven GPS data collection system for studying ionosphere scintillation," MS thesis, Miami University, Department of Electrical and Computer Engineering, 2011.

[8]. Peng, S., Y. Morton, "A USRP2-based reconfigurable multi-constellation multi-frequency GNSS software receiver front end," GPS Solutions, under revision.

[9]. https://www.ettus.com/product

[10]. https://www.ettus.com/product/category/Daughterboards

[11]. Misra, P. and P. Eng, "Global Positioning System: Signals, Measurements, and Performance," Ganga-Jamuna Press, Second Edition, 2006.

[12]. Van Dierendonck, A.J., "GPS Receivers," in Global Positioning System: Theory and Applications," Vol.I, Parkinson, B.W. and Spilker, J.J. Jr., eds., AIAA, 1996, pp. 329-407.

[13]. Gunawardena, S., Z. Zhu, F. van Graas, "Triple Frequency RF Front-End for GNSS Instrumentation Receiver Applications," Proc. ION GNSS, Savana, GA, Sept. 2008.